DOI: 10.1002/chem.200700896

Fe_2 and Fe_4 Clusters Encapsulated in Vacant Polyoxotungstates: Hydrothermal Synthesis, Magnetic and Electrochemical Properties, and DFT Calculations

Céline Pichon,[a] Anne Dolbecq,*[a] Pierre Mialane,[a] Jérôme Marrot,[a] Eric Rivière,[b] Monika Goral,[c] Monika Zynek,[c] Timothy McCormac,[c] Serguei A. Borshch,[d] Ekaterina Zueva,[e] and Francis Sécheresse[a]

Abstract: While the reaction of $[PW_{11}O_{39}]^{7-}$ with first row transition-metal ions M^{n+} under usual bench conditions only leads to monosubstituted $\{PW_{11}O_{39}M(H_2O)\}$ anions, we have shown that the use of this precursor under hydrothermal conditions allows the isolation of a family of novel polynuclear discrete magnetic polyoxometalates (POMs). The hybrid asymmetric $[Fe^{II}(bpy)_3][PW_{11}O_{39}Fe_2^{III}(OH)(bpy)_2]\cdot 12H_2O$ (bpy = bipyridine) complex (**1**) contains the dinuclear {Fe(μ-O(W))(μ-OH)Fe} core in which one iron atom is coordinated to a monovacant POM, while the other is coordinated to two bipyridine ligands. Magnetic measurements indicate that the Fe^{III} centers in complex **1** are weakly antiferromagnetically coupled ($J = -11.2\ cm^{-1}$, $H = -JS_1S_2$) compared to other {Fe(μ-O)(μ-OH)Fe} systems. This is due to the long distances between the iron center embedded in the POM and the oxygen atom of the POM bridging the two magnetic centers, but also, as shown by DFT calculations, to the important mixing of bridging oxygen orbitals with orbitals of the POM tungsten atoms. The complexes $[Hdmbpy]_2[Fe^{II}(dmbpy)_3]_2[(PW_{11}O_{39})_2Fe_4^{III}O_2(dmbpy)_4]\cdot 14H_2O$ (**2**) (dmbpy = 5,5′-dimethyl-2,2′-bipyridine) and $H_2[Fe^{II}(dmbpy)_3]_2[(PW_{11}O_{39})_2Fe_4^{III}O_2(dmbpy)_4]\cdot 10H_2O$ (**3**) represent the first butterfly-like POM complexes. In these species, a tetranuclear Fe^{III} complex is sandwiched between two lacunary polyoxotungstates that are pentacoordinated to two Fe^{III} cations, the remaining paramagnetic centers each being coordinated to two dmbpy ligands. The best fit of the $\chi_M T = f(T)$ curve leads to $J_{wb} = -59.6\ cm^{-1}$ and $J_{bb} = -10.2\ cm^{-1}$ ($H = -J_{wb}(S_1S_2 + S_1S_{2*} + S_{1*}S_2 + S_{1*}S_{2*}) - J_{bb}(S_2S_{2*})$). While the J_{bb} value is within the range of related exchange parameters previously reported for non-POM butterfly systems, the J_{wb} constant is significantly lower. As for complex **1**, this can be justified considering Fe_w–O distances. Finally, in the absence of a coordinating ligand, the dimeric complex $[N(CH_3)_4]_{10}[(PW_{11}O_{39}Fe^{III})_2O]\cdot 12H_2O$ (**4**) has been isolated. In this complex, the two single oxo-bridged Fe^{III} centers are very strongly antiferromagnetically coupled ($J = -211.7\ cm^{-1}$, $H = -JS_1S_2$). The electrochemical behavior of compound **1** both in dimethyl sulfoxide (DMSO) and in the solid state is also presented, while the electrochemical properties of complex **2**, which is insoluble in common solvents, have been studied in the solid state.

Keywords: density functional calculations · electrochemistry · hydrothermal synthesis · magnetic properties · polyoxometalates

[a] C. Pichon, Dr. A. Dolbecq, Dr. P. Mialane, Dr. J. Marrot, Prof. F. Sécheresse
Institut Lavoisier, IREM, UMR 8180
Université de Versailles Saint-Quentin en Yvelines
45 Avenue des Etats-Unis, 78035 Versailles cedex (France)
Fax: (+33) 139-254-381
E-mail: dolbecq@chimie.uvsq.fr

[b] Dr. E. Rivière
Institut de Chimie Moléculaire et des Matériaux d'Orsay
UMR 8182, Equipe Chimie Inorganique
Univ Paris-Sud, 91405 Orsay (France)

[c] M. Goral, M. Zynek, Dr. T. McCormac
Centre for Research in Electroanalytical Technology "CREATE"
Institute of Technology Tallaght
Department of Science, Dublin 24 (Ireland)

[d] Dr. S. A. Borshch
Laboratoire de Chimie, UMR 5182
Ecole Normale Supérieure de Lyon
46 Allée d'Italie, 69364 Lyon Cedex 07 (France)

[e] Dr. E. Zueva
Department of Inorganic Chemistry
Kazan State Technological University, Kazan, 420015 (Russia)

Supporting information for this article is available on the WWW under http://www.chemeurj.org/ or from the author.

Introduction

The architectures of most polyoxometalates (POMs) are based on specific structural types, such as the Lindquist (e.g. $[W_6O_{19}]^{2-}$), Keggin (e.g. $[PW_{12}O_{40}]^{3-}$), or Dawson (e.g. $[P_2W_{18}O_{62}]^{6-}$),[1] although POMs with new topological arrangements are still being discovered.[2] Lacunary polyoxotungstates act as ligands that can bind to 3d transition-metal ions giving rise to species containing transition-metal clusters with nuclearities from 1 to 28[3] and exhibiting appealing properties particularly in the fields of molecular magnetism[4] and catalysis.[5] Furthermore, the incorporation of exogeneous ligands bridging the paramagnetic centers allows the magnetic coupling between the transition-metal ions encapsulated within the POM to be modulated.[6] Most of these POM compounds are synthesized by the direct reaction of the lacunary precursor with transition-metal ions under mild conditions (ambient pressure, $T<100\,^{\circ}C$). The use of hydrothermal conditions with preformed POMs as precursors has so far been limited to mainly saturated Keggin anions such as $[SiW_{12}O_{40}]^{4-}$, leading to materials with isolated transition-metal ions.[7] A rare example of a vacant POM introduced in a hydrothermal reactor, $[SiW_{10}O_{36}]^{8-}$, has led to the neutral molecular complex $[Cu_2(O_2CMe)_2$(5,5′-dimethyl-2,2′-bpy)$_2][Cu$(5,5′-dimethyl-2,2′-bpy)$_2][SiW_{12}O_{40}]$ (bpy = bipyridine), because of the instability of the lacunary precursor.[8] It is only very recently that the first example of the successful use of lacunary POMs as precursors (i.e., with conservation of the introduced lacunary POM ligand) has been reported, affording monomeric hexanuclear clusters.[9] On the other hand, numerous structures of polyoxotungstates synthesized with Na_2WO_4 as a precursor and under hydrothermal conditions have been described in the last few years, giving access to materials based on isopolyoxotungstates,[10] phosphotungstates,[10b,11] germanotungstates,[12] and silicotungstates[10b,11d,13] building units, according to the presence or absence of a heteroelement. It should be noted that when tungstate is used as a precursor in such conditions, so far it has been difficult, if at all possible, to control the nature of the resulting POM ligand. Moreover, in most cases, saturated POM systems are obtained. Concerning the nature of the 3d transition metal used, numerous heteropolyoxotungstate-based materials incorporate copper ions. This can be related to the Jahn–Teller effect in Cu^{II} complexes that permits diverse connecting modes between the POMs and the 3d center. However, to our knowledge, only one example of an iron-containing POM system synthesized under hydrothermal conditions, a $[PW_{12}O_{40}]^{3-}$ ion with a $\{Fe^{II}(phen)_2(H_2O)\}$ group, has been reported,[14] while the synthesis of iron-based POM materials has been extensively explored under normal bench conditions. These multi-iron complexes exhibit spectacular structures[3] and appealing magnetic[15] or electrochemical properties; [16] they are also interesting because of their catalytic properties,[17] including biomimetic catalysis. Indeed, POMs can be seen as rigid polydentate ligands with electron-acceptor properties similar to the active sites of natural enzymes.[18]

We have, thus, decided to explore the reactivity of preformed vacant POMs with iron(III) ions under hydrothermal conditions, and we report our first results with monolacunary $[PW_{11}O_{39}]^{7-}$ ions as the building units in the presence or absence of organic ligands. A unique asymmetric dibridged, dinuclear Fe^{III} complex, in which one metal center is embedded in a $[PW_{11}O_{39}]^{7-}$ unit, while the other is connected to bipyridine ligands, has been characterized. The value of the exchange coupling parameter between the two paramagnetic centers has been experimentally quantified and was found to be surprisingly low. This result has been rationalized by using DFT calculations. The first butterfly-like POM complex which can be seen as the condensation product of two units similar to the dinuclear complex mentioned above has also been obtained. The magnetic properties of this compound have been compared to those found in previously reported organic-ligand/Fe^{III} butterfly systems. Finally, in the absence of an organic ligand, a purely inorganic dinuclear Fe^{III} polyoxometalate in which the two iron centers are very strongly antiferromagnetically coupled has been characterized. The electrochemical properties of the hybrid species are also reported.

Results and Discussion

Syntheses, IR spectroscopy, TG analysis, and X-ray powder diffraction: Dark red crystals of $[Fe^{II}(bpy)_3][PW_{11}O_{39}Fe_2^{III}(OH)(bpy)_2]\cdot 12H_2O$ (**1**) were obtained in high yield by the reaction of $[\alpha\text{-}PW_{11}O_{39}]^{7-}$, $Fe_2(SO_4)_3$, and 2,2′-bpy in a ratio of 1:1.5:5 in water at 160 °C. A slight modification of the organic ligand led to a dimerization of the anionic unit. Hence, $(Hdmbpy)_2[Fe^{II}(dmbpy)_3]_2[(PW_{11}O_{39})_2Fe_4^{III}O_2(dmbpy)_4]\cdot 14H_2O$ (**2**) has thus been isolated in conditions similar to **1** except that 5,5′-dimethyl-2,2′-bipyridine (dmbpy) was used instead of 2,2′-bipyridine. When the quantity of organic ligand was lowered, other parameters remained unchanged, only the nature of the counter cations was modified. Two protons replaced two protonated $Hdmbpy^+$ cations to give $H_2[Fe^{II}(dmbpy)_3]_2[(PW_{11}O_{39})_2Fe_4^{III}O_2(dmbpy)_4]\cdot 10H_2O$ (**3**). Finally, when non-coordinating tetramethylammonium cations were introduced in the synthetic medium in place of the chelating bpy ligands, the dimeric compound $[N(CH_3)_4]_{10}[(PW_{11}O_{39}Fe^{III})_2O]\cdot 12H_2O$ (**4**) crystallized. We have studied the influence of synthetic parameters on the obtained compounds:

1) *pH*: Complexes **1–4** are only obtained in a limited pH domain, around 3. When the pH is too low, the monovacant POM is unstable and gives the saturated $[PW_{12}O_{40}]^{3-}$ ion. Preliminary X-ray diffraction studies[19] suggest that the crystals isolated with the experimental conditions used for **2**, except that the initial pH was 2, contain $[PW_{12}O_{40}]^{3-}$ ions and $[Fe^{II}(dmbpy)_3]^{2+}$ counterions. At higher pH values, the yield and the crystallinity of complexes **1–4** are lowered.

2) *Precursors*: First, it can be noted that complex **1** was primarily obtained by the reaction of $[A\text{-}\alpha\text{-}PW_9O_{34}]^{9-}$, showing the instability of this precursor under such conditions. Secondly, considering that the counterion in complexes **1**, **2**, and **3** is the $[Fe^{II}(bpy)_3]^{2+}$ complex (see below) although only $Fe_2(SO_4)_3$ was used as a reactant, we have performed the same experiments using a mixture of 1) $Fe_2(SO_4)_3$ and $FeSO_4$ or 2) $Fe_2(SO_4)_3$ and preformed $[Fe^{II}(bpy)_3]^{2+}$ ($[Fe^{III}]/[Fe^{II}]=2$) as iron precursors. It has been possible to isolate only **1** by this alternative procedure, but neither the yield nor the crystallinity was improved.
3) *Temperature and pressure*: We have tried to synthesize complexes **1**–**4** using conventional methods. For these experiments, the heterogeneous mixture containing the reactants was introduced to a round-bottomed flask and refluxed for 24 h in an oil bath. After cooling to room temperature, the solution was filtered, and the amorphous powder was dried. In all the cases, we have found that hydrothermal conditions were the only way to obtain complexes **1**–**4**.

These experiments show that only a precise set of parameters allow the synthesis of crystalline compounds **1**–**4**. Different phases that could not be characterized by single-crystal X-ray diffraction have been obtained by a slight variation of the parameters. Among them may exist the one-dimensional chain of monosubstituted Keggin anions linked through Fe-O-W bridges, which has already been described for the Mn^{II}[20] and Co^{II}[21] derivatives.

Complexes **1** and **4** are slightly soluble in DMSO (dimethyl sulfoxide), while **2** and **3** are completely insoluble in common solvents.

The infrared (IR) spectra of complexes **1**–**4** were recorded between 4000 and 400 cm^{-1}. Compounds **2** and **3**, differing only by the presence of protons, have almost identical infrared spectra, while the spectra of **1**, **2**, and **4** exhibit slight differences in the 1100–400 cm^{-1} region (Figure SI1 in the Supporting Information). The splitting ($\Delta\nu$) of the asymmetric P–O stretching vibration of the distorted central PO_4 tetrahedron is more pronounced in complex **4** (1093, 1057, $\Delta\nu=36\ cm^{-1}$) than in complex **2** (1084, 1064, $\Delta\nu=20\ cm^{-1}$) and complex **1** (1075, 1066, $\Delta\nu=9\ cm^{-1}$). Usually, the splitting of the asymmetric P–O stretching vibration in a monosubstituted $\{PW_{11}M\}$ anion is related to the strength of the M–O(PO_3) bond. The splitting is thus maximal for $M=Cu^{II}$ (1105, 1065, $\Delta\nu=40\ cm^{-1}$) and closest to the splitting observed in $[PW_{11}O_{39}]^{7-}$ (1085, 1040, $\Delta\nu=45\ cm^{-1}$).[22] The splitting in complex **4** is thus close to the largest splittings observed in the family of monosubstituted lacunary derivatives. The splitting in complex **2** is more along the order of the values reported for $[PW_{11}O_{39}Fe^{III}(H_2O)]^{4-}$ (1084, 1060, $\Delta\nu=24\ cm^{-1}$),[23] and the splitting in complex **1** is close to the zero splitting value of the saturated $[PW_{12}O_{40}]^{3-}$ anion. The increasing value of $\Delta\nu$ from complexes **1** to **4** can be tentatively explained by weaker interactions between the metal and the POM as shown by the significant elongation of the Fe–O(PO_3) bond from complex **1** to complex **4** (Table 1, see also the structural description below).

Table 1. Selected bond lengths [Å] and angles [°] in complexes **1**, **2**, and **4** associated to the representations in Figures 1 and 2.

Compound **1**			
Fe1–O14	1.905(11)	Fe2–O7	1.915(11)
Fe1–O37	1.925(11)	Fe2–O9	1.941(12)
Fe1–O9	1.932(12)	Fe2–N2	2.104(13)
Fe1–O10	1.992(11)	Fe2–N3	2.109(14)
Fe1–O7	2.106(11)	Fe2–N4	2.151(16)
Fe1–O25	2.271(11)	Fe2–N1	2.157(14)
Fe1–Fe2	3.013(3)		
Fe2-O7-Fe1	97.05(5)	Fe1-O9-Fe2	102.1(5)
Compound **2**			
Fe1–O40	1.926(9)	Fe2–O40	1.929(7)
Fe1–O36	1.944(11)	Fe2–O40	1.943(11)
Fe1–O39	1.955(9)	Fe2–N12	2.152(8)
Fe1–O27	2.007(10)	Fe2–N15	2.158(6)
Fe1–O23	2.030(10)	Fe2–N1	2.186(13)
Fe1–O25	2.472(10)	Fe2–N26	2.215(8)
Fe1–Fe2	3.491(5)	Fe2–Fe2	2.910(4)
Fe2-O40-Fe1	133.6(6)	Fe2-O40-Fe2*	97.4(4)
Fe1-O40-Fe2	129.0(4)		
Compound **4**			
Fe1–O79	1.775(7)	Fe2–O79	1.767(7)
Fe1–O39	1.988(8)	Fe2–O47	1.969(8)
Fe1–O17	1.999(9)	Fe2–O70	1.976(9)
Fe1–O9	2.001(8)	Fe2–O53	2.002(9)
Fe1–O30	2.029(9)	Fe2–O78	2.010(8)
Fe1–O11	2.616(8)	Fe2–O57	2.594(9)
Fe1–Fe2	3.513(3)		
Fe2-O79-Fe1	165.4(6)		

Thermogravimetric analysis (TGA) was performed and showed similar behaviors for the four compounds (Figure SI2 in the Supporting Information) and confirmed 1) the number of hydration water molecules, 2) the number of bpy ligands on complexes **1**–**3**, and 3) the number of TMA^+ (TMA = tetramethyl ammonium) counterions in complex **4**. In the TGA, the first loss corresponds to the departure of water molecules. For complexes **1**–**3**, upon further heating, a two-step weight loss was observed between 300 and 800 °C with a total weight loss corresponding to the departure of the bpy molecules. Such a two-step departure of 2,2′-bpy ligands has been previously observed and attributed to the retention of carbon from the calcination of bpy, the carbon being only slowly removed from the solid residue.[24]

A comparison of the experimental X-ray diffraction powder patterns of the four compounds and of the powder patterns calculated from the structure solved from single-crystal X-ray diffraction data is given as Supporting Information (Figure SI3) and confirms the bulk compositions.

Structural analysis: Complexes **1**–**3** are molecular compounds with substituted POM anions and monomeric iron complexes bound to bpy ligands as counter-cations. Although the iron precursor contains Fe^{III} ions, it is doubtless that the cations are low spin $[Fe^{II}(bpy)_3]^{2+}$ complexes for three main reasons: 1) the reduction of $[Fe^{III}(bpy)_3]^{3+}$ to

$[Fe^{II}(bpy)_3]^{2+}$ by water has been known for a long time and a mechanism has been proposed,[25] 2) the charge of the counter-cations is consistent with the results of elemental analyses and electroneutrality considerations, and 3) magnetic measurements indicate that for complexes **1**–**3** the counter- ions are diamagnetic (see below).

In complex **1**, the anion (Figure 1a) can be described as a dissymmetric dinuclear Fe_2 complex. The Fe1 ion is bound to the pentadentate monolacunary $[PW_{11}O_{39}]^{7-}$ anion, and

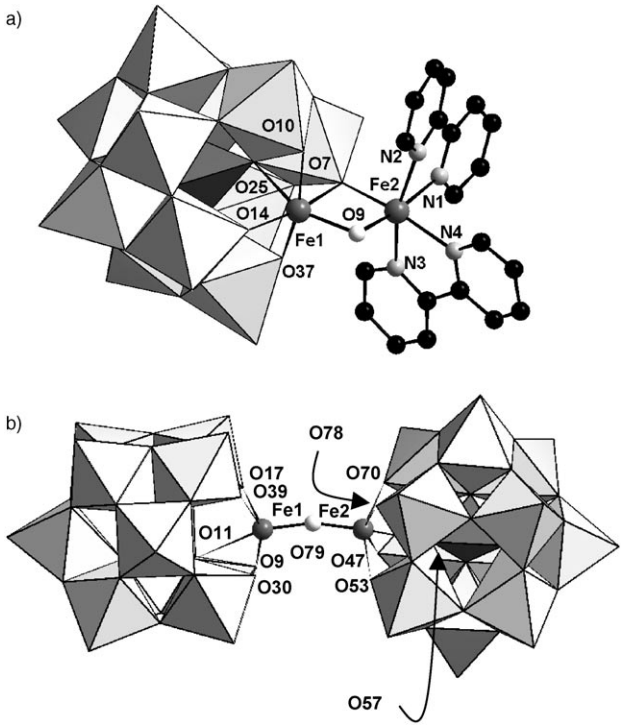

Figure 1. a) Mixed ball and stick and polyhedral representation of the $[PW_{11}O_{39}Fe_2^{III}(OH)(bpy)_2]^{2-}$ anion in **1**; white octahedra WO_6, dark gray tetrahedron PO_4, medium gray spheres Fe, white spheres O, light gray spheres N, black spheres C; b) mixed ball and stick and polyhedral representation of the $[(PW_{11}O_{39})_2Fe_2^{III}O]^{10-}$ anion in **4**; white octahedra WO_6, dark gray tetrahedra PO_4, medium gray spheres Fe, white spheres O.

the Fe2 ion is linked to two 2,2′-bpy ligands. Fe1 and Fe2 are bridged by two oxygen atoms, O7 is the oxygen atom from the O=W group of the POM ligand and O9 belongs to a hydroxo ligand as indicated by valence-bond calculations ($\Sigma s = 1.23$).[26] Valence-bond calculations also confirm the valence of Fe1 ($\Sigma s = 3.11$), but it should be noted that these calculations are not conclusive for ions bound to bpy ligands. The $Fe1O_6$ octahedron is highly distorted in the equatorial plane with the Fe1–O7 distance far longer than the three other Fe–O distances. The axial Fe–O(PO_3) distances are also elongated (Table 1).

As the same anion is found in both the structures of complex **2** and complex **3**, its description will only be given for **2**. This anion (Figure 2a) can be viewed as the condensation of two of the anions present in complex **1**. By using the labeling scheme adopted for compound **1** (Figure 1a), this

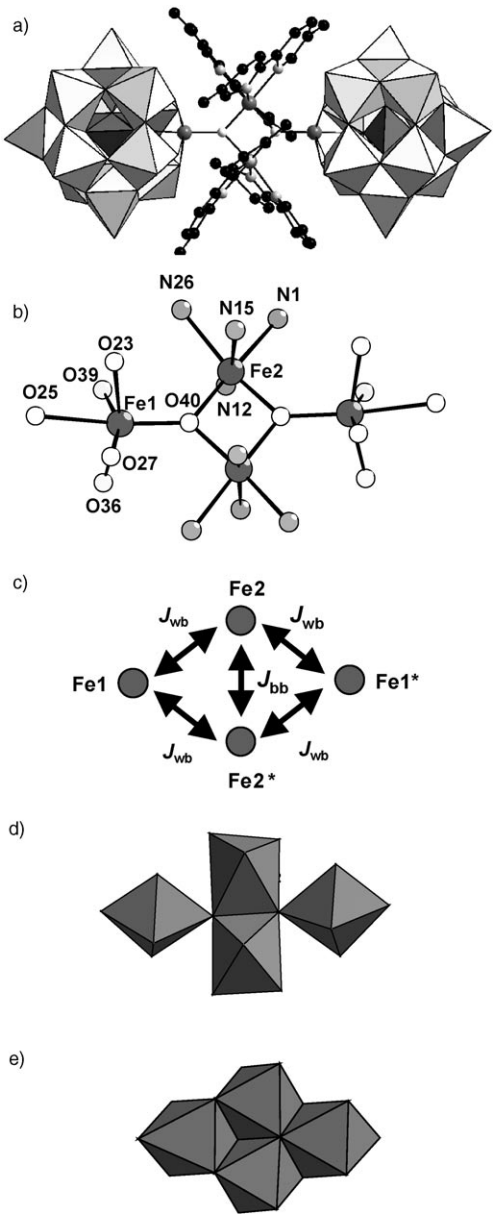

Figure 2. a) Mixed ball and stick and polyhedral representation of the $[(PW_{11}O_{39})_2Fe_4^{III}O_2(dmbpy)_4]^{6-}$ anion common in **2** and **3**; white octahedra WO_6, dark gray tetrahedra PO_4, medium gray spheres Fe, white spheres O, light gray spheres N, black spheres C; b) view of the tetrameric butterfly complex sandwiched between the two monolacunary anions with atom labeling scheme; the carbon atoms of the organic ligand have been omitted for clarity; c) schematic representation of the Fe_4 core showing the two main exchange interactions, the star indicates symmetry related atoms; d) polyhedral representation of the Fe_4 core in complex **2**; e) polyhedral representation of the rhombohedral M_4 magnetic clusters prepared from trivacant POMs.

condensation can be seen as resulting from the breaking of the Fe2–O7 bond and the concomitant formation of a Fe2–O9 bond with a neighboring anion. The tetranuclear Fe_4 complex encapsulated between the two POMs belongs to a well-known family of butterfly complexes.[27] The Fe2–Fe2* fragment (Figure 2b) features the body of the butterfly, and the Fe2-Fe1-Fe2* and Fe2-Fe1*-Fe2* triangles schematize

the wings, with the Fe1 and Fe1* ions thus occupying the "wingtip" positions. The dihedral angle between the least-squares planes defined by the Fe1/Fe2/Fe2* and Fe1*/Fe2/Fe2* ions is 175.5°, thus the four Fe^{III} ions are essentially coplanar. The sum of the Fe-O-Fe angles around the μ_3-O O40 atom is equal to the ideal value of 360°. The geometry of the tetranuclear Fe_4 core in the butterfly complex thus differs from that of the more familiar rhombohedral M_4 magnetic clusters[28] prepared from trivacant POMs such as $[M^{II}_4(H_2O)_2(B\text{-}\alpha\text{-}PW_9O_{34})_2]^{10-}$ (M = Co, Cu, Zn, Mn)[29] and $[M^{III}_4(H_2O)_2(B\text{-}\alpha\text{-}PW_9O_{34})_2]^{6-}$ (M = Fe).[30] These complexes contain four coplanar MO_6 octahedra sharing edges (Figure 2e). In the butterfly complex, the two edge-sharing octahedra of the body share only one corner with the octahedra of the wings (Figure 2d). Valence-bond calculations indicate that O40 ($\Sigma s = 1.88$) is an oxo ligand and confirm the valence of Fe1 ($\Sigma s = 2.97$). The $Fe1O_6$ octahedron is more axially distorted in complex **2** than in complex **1** (Table 1), that is, the interaction of the Fe1 ion with the monolacunary POM is weaker in complex **2** than in complex **1** which is expressed in the infrared spectra (see above).

In complex **4**, the anion results from the dimerization of two $[PW_{11}O_{39}Fe^{III}(H_2O)]^{4-}$ ions (Figure 1b). In the dimer, the Fe^{III} centers encapsulated in the vacant POMs are bridged by a single oxo ligand as indicated by valence-bond calculations ($\Sigma s = 1.94$), which also confirm the +3 oxidation state of the metallic centers ($\Sigma s = 3.12$ for Fe1 and 3.23 for Fe2). The dimerization of $[PW_{11}O_{39}Fe^{III}(H_2O)]^{4-}$ leading to $[\{PW_{11}O_{39}Fe^{III}\}_2O]^{10-}$ has been previously evidenced in aqueous solution, but it had not been possible to isolate and characterize the dimer in the solid state.[31] The dimerization of transition-metal mono-substituted POMs has also been studied for the titanium (in organic medium),[32] zirconium[33] and ruthenium[34] derivatives, but the structural characterization of a μ-oxo bridged dimer has only very recently been performed in the case of $[\{SiW_{11}O_{39}Ru^{IV}\}_2O]^{10-}$.[34b] As observed in this latter compound, the dimeric anion in complex **1** does not possess a symmetry element. The axial distortion of the FeO_6 octahedra in complex **4** is still higher than that observed in complex **2** (Table 1). The Fe^{III}-O-Fe^{III} angle (165°) is larger than the Ru^{IV}-O-Ru^{IV} bridging angle (154°) in $[\{SiW_{11}O_{39}Ru^{IV}\}_2O]^{10-}$.

Magnetic properties: The magnetic behavior of **1** was investigated between 2 and 300 K and is shown as $\chi_M T$ versus T (Figure 3), with χ_M being the magnetic susceptibility for one mole of complex **1**. The $\chi_M T$ value at room temperature (7.30 $cm^3 mol^{-1} K$) is lower than the calculated $\chi_M T$ value of 8.75 $cm^3 mol^{-1} K$ for two noninteracting high-spin Fe^{III} centers with $g = 2.00$. The $\chi_M T$ curve decreases continuously upon sample cooling, reaching a $\chi_M T$ value of 0.40 $cm^3 mol^{-1} K$ at 2 K. This behavior is characteristic of an antiferromagnetic interaction with a diamagnetic ground state. The $\chi_M T$ curve was fitted with the Bleaney–Bowers equation derived from the Heisenberg–Dirac–van Vleck (HDVV) Hamiltonian $H = -JS_1S_2$ with $S_1 = S_2 = 5/2$ associated with the two interacting Fe^{III} centers within the dinuclear

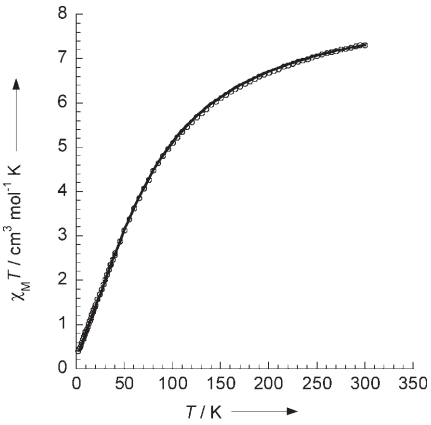

Figure 3. Plot of $\chi_M T$ versus T for compound **1** between 300 and 2 K. The solid line was generated from the best fit parameters given in the text.

cluster. The best fit parameters obtained are $J = -11.2\ cm^{-1}$ and $g = 1.98$ ($R = 4.8\ 10^{-6}$).[35] Dinuclear iron complexes with oxo, hydroxo, peroxo, or carboxylato bridges continue to attract much attention, mainly as models of metalloenzymes, and their magnetic properties have been widely studied.[36] Diferric complexes with Fe^{III}(μ-O)(μ-OH)Fe^{III} cores are antiferromagnetically coupled with a J value around $-100\ cm^{-1}$,[37] far larger than the value determined in complex **1**. The J value in complex **1** is thus more along the order of the J values observed for dibridged diferric complexes with one μ-OH ligand, the second bridge being an hydroxo, an alkoxo, or a phenolato ligand.[36a] The present result confirms that the exchange interactions mediated through oxygen atoms connected to tungsten centers are very weak, and hence much weaker than those commonly observed in μ-O bridged compounds. Focusing on iron systems, it has been shown that for supported[38] and unsupported[39] oxo bridged compounds the Fe–O distance is the main parameter which governs the strength of the magnetic interaction. In complex **1**, the Fe-(μ-O(POM)) distances are long (1.915(11) and 2.106(11) Å) compared to those classically found in dinuclear μ-O bridged Fe^{III} complexes, which justifies the low J value determined for this compound. DFT calculations on complex **1** have been performed in order to clarify this point (see below).

As the magnetic clusters in complexes **2** and **3** are similar, the magnetic data were recorded only on a sample of complex **2**. The $\chi_M T$ value at room temperature (4.3 $cm^3 mol^{-1} K$) is far lower than the calculated $\chi_M T$ value of 17.5 $cm^3 mol^{-1} K$ for four noninteracting high spin Fe^{III} centers (assuming $g = 2.00$), indicating relatively strong antiferromagnetic interactions (Figure 4a). This is also shown by the continuous decrease of the $\chi_M T$ curve upon sample cooling. As already mentioned, the Fe_4 core in complex **2** belongs to the known class of butterfly complexes. In these compounds, a rigorous interpretation would imply the consideration of three J values: J_{wb} between one body iron and one external atom, J_{ww} between the two wingtip iron atoms, and J_{bb} between the two body iron atoms (Figure 2c). However, considering that the J_{wb} exchange parameter must be

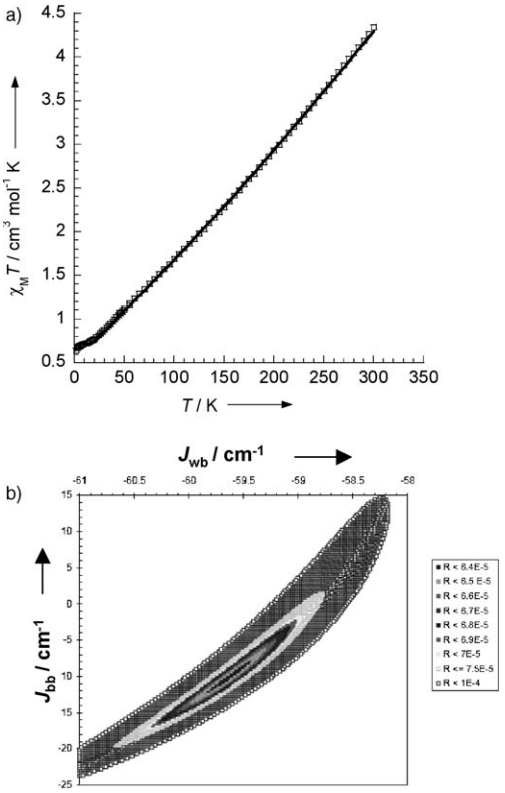

Figure 4. a) Plot of $\chi_M T$ versus T for compound **2** between 300 and 2 K. The solid line was generated from the best fit parameters given in the text; b) error contour plots for different J_{wb} and J_{bb} values for the simulation of the magnetic susceptibility measurement of complex **2**.

weaker than J_{bb} and J_{ww} due to the long Fe1···Fe1 distance, only J_{bb} and J_{ww} are usually considered. This also avoids overparametrization. The corresponding Hamiltonian for this model is expressed in Equation (1) with $S_1 = S_2 = S_{1*} = S_{2*} = 5/2$.

$$H = -J_{wb}(S_1S_2 + S_1S_{2*} + S_{1*}S_2 + S_{1*}S_{2*}) - J_{bb}(S_2S_{2*}) \qquad (1)$$

A best fit of the experimental $\chi_M T$ curve gave $J_{wb} = -59.6\ cm^{-1}$ and $J_{bb} = -10.2\ cm^{-1}$, assuming $g = 2.00$ ($R = 6.31\ 10^{-5}$).[35] As usually observed, the J_{wb} coupling constant is antiferromagnetic and corresponds to the strongest interaction.[40] With respect to other butterfly compounds,[40] this value is the smallest observed value ($-92.0 \le J_{wb} \le -65.7\ cm^{-1}$), and this can again be correlated to long Fe_w–O distances (1.93 Å in complex **2**, $1.81 \le Fe_w\text{–}O \le 1.89$ Å in compounds reported in the literature), Fe_w is the iron center of the wing. The J_{bb} coupling constant is weakly antiferromagnetic, but it should be noted that similarly satisfactory fits could be obtained for $-12 < J_{bb} < -8\ cm^{-1}$, as shown by the error contour plot in Figure 4b. On the other hand, only values of J_{wb} close to $-59.6\ cm^{-1}$ give low R values (Figure 4b). This lack of definition of J_{bb} has already been discussed and has been related to spin frustration of the centered spins.[27a–c] The J_{bb} value is in the range of the previously reported values ($-21.8 \le J_{bb} \le -2.4\ cm^{-1}$), but its absolute value is significantly lower than those found for the recently reported compound $[Fe_4O_2Cl_2(O_2CMe)\{(py)_2CNO\}_4]$ ($(py)_2$-CNO = di-2-pyridyl ketone oxime, $J_{bb} = -59.4\ cm^{-1}$),[27d] which possesses a triplet ground state, thus confirming that the ground state in complex **2** is diamagnetic.

As expected for a Fe-O-Fe dimer, the two Fe^{III} centers are strongly antiferromagnetically coupled in complex **4** as shown (Figure 5) by 1) the low $\chi_M T$ value at room temperature ($0.85\ cm^3\,mol^{-1}\,K$), which is more than ten times lower than the calculated $\chi_M T$ value of $8.75\ cm^3\,mol^{-1}\,K$ for two noninteracting high-spin Fe^{III} centers (assuming $g = 2.00$) and 2) the strong J value of $-211.7\ cm^{-1}$ determined by fitting the $\chi_M T$ curve with the Bleaney–Bowers equation derived from the HDVV Hamiltonian $H = -JS_1S_2$ with $S_1 = S_2 = 5/2$, assuming $g = 2.00$ ($R = 4\ 10^{-5}$).[35] The J value in **4** falls in the range of the J values determined for single oxo-bridged diiron(III) complexes ($-240 < J < -160\ cm^{-1}$),[36] confirming the protonation degree of the oxygen atom connected to the two $\{PW_{11}O_{39}Fe^{III}\}$ sub-units.

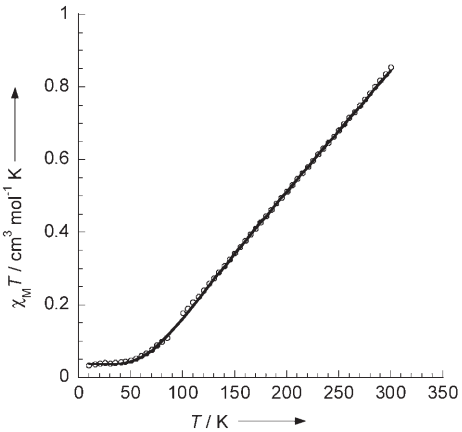

Figure 5. Plot of $\chi_M T$ versus T for compound **4** between 300 and 2 K. The solid line was generated from the best fit parameters given in the text.

DFT calculations: The DFT calculations of the exchange parameter for cluster **1** containing two paramagnetic Fe^{III} centers were performed to determine the role of different structural and electronic factors. First, the calculations were done for cluster **1** at the experimentally found geometry. As usual in the broken-symmetry DFT method, two states were calculated, namely the high-spin (HS) state with the total spin $S = 5$ and the broken-symmetry (BS) state. The exchange parameter was estimated through the expression derived by Yamaguchi $J = 2(E_{BS}\text{-}E_{HS})/(\langle S^2\rangle_{HS} - \langle S^2\rangle_{BS})$. We obtained $J = -12\ cm^{-1}$, which is very close to the experimentally observed value $-11.2\ cm^{-1}$. To compare this case with the situation in diiron(III) complexes with one μ-oxo and one μ-hydroxo bridge, we also performed calculations for the model dinuclear complex $[Fe_2^{III}(\mu\text{-}O)(\mu\text{-}OH)(bpy)_4]^{3+}$. The structure of the model complex was optimized for its HS state. The calculations again led to an antiferromagnetic interaction between Fe^{III} ions with $J = -68\ cm^{-1}$, which is

much stronger than for the polyoxometalate encapsulated dimer. Nevertheless, this value corresponds more to the range characteristic for dibridged iron complexes (see above). The main reasons for such a difference can be looked for in the geometry of the $\{Fe_2^{III}(\mu\text{-}O)(\mu\text{-}OH)\}$ core. Due to the bond with the polyoxometalate tungsten atom, the bridging oxygen atom in complex **1** is well separated from the Fe1 atom (2.106 Å), and the distance to Fe2 is equal to 1.915 Å. In the symmetric model complex, both distances are equal to 1.90 Å. Different hypotheses can be found in the literature concerning magnetostructural correlations in oxo-bridged iron(III) dimers. In some works, *J* values for asymmetric complexes were correlated with the mean Fe–O distance,[38] whereas the correlation with the longest Fe–O distance was also proposed.[41] In any case, the changes in the geometry of the Fe-O-Fe linkage between the model complex and complex **1** must lead to a weakening of the magnetic interaction. Another factor, which could also be responsible for the variation in the exchange couplings, is the important mixing of magnetic orbitals. This mixing is composed of 3d iron orbitals with participation from 2p bridging oxygen orbitals, and with 5d orbitals of polyoxometalate tungsten atoms linked to μ-oxo bridges. The latter enter into the magnetic orbitals with about the same weight as iron orbitals. This situation differs from the earlier considered case of diiron substituted γ-Keggin silicotungstates,[42] where magnetic orbitals are only slightly mixed with tungsten orbitals (see Figure 6 and Table 7 in reference [37]) and the variation of exchange parameters between the polyoxometalate and a simple dimer is much less pronounced.

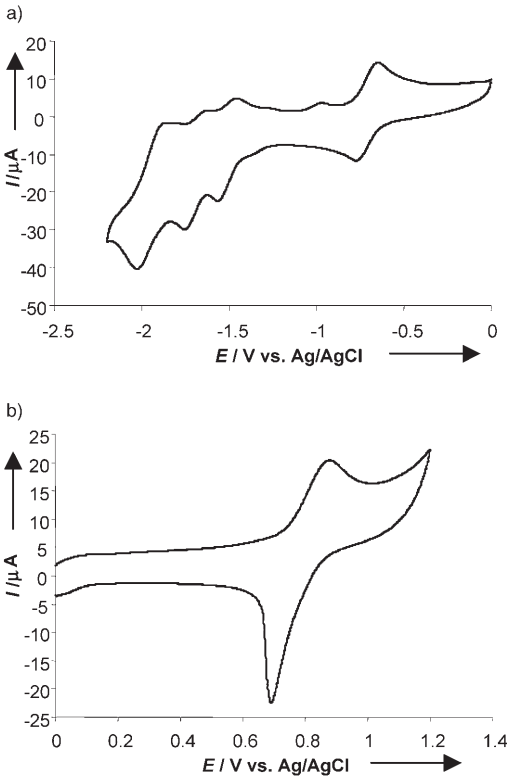

Figure 6. Cyclic voltammograms of a 2 mM solution of complex **1** in 0.1 M NH_4PF_6 at a bare carbon electrode ($A = 0.0707\ cm^2$) a) in the −2.5 to 0.0 V range; b) in the 0.0–1.4 V range. Scan rate = 100 mV s^{-1}.

Electrochemical properties: Attempts were made to elucidate the redox properties of the two complexes (**1** and **2**) both in solution and in the solid state. The limited solubility of both complexes placed restrictions upon the solution phase investigations. Our interest was to see if redox activity for the Fe^{III} centers and W–O framework for the POM complexes could be observed. The cyclic voltammogram obtained for a solution of complex **1** in a 0.1 M NH_4PF_6 DMSO (Figure 6) showed a series of redox processes associated with the $Fe^{III/II}$ and bipyridine ligands of the $[Fe(bpy)_3]^{2+}$ moiety. The three monoelectronic bipyridine-based redox processes were located at −1.515, −1.699, and −1.946 V (vs. Ag/AgCl) with the $Fe^{III/II}$ at +0.780 V (vs. Ag/AgCl). These are in close agreement with $[Fe(bpy)_3][PF_6]_2$ under the same experimental conditions, as seen in Figure SI4 in the Supporting Information. A single redox process at an $E_{1/2}$ of approximately −0.771 V versus Ag/AgCl (Figure 6a) was also observed. When compared to the Fe^{III} Keggin parent POM $[PW_{11}O_{39}Fe^{III}(H_2O)]^{4-}$ under the same solution conditions, this redox couple can be attributed to the Fe^{III} center substituted into the POM cage. It was not possible, however, to view the redox switching of the other Fe^{III} site within the compound or the W–O framework in solution. As a result, solid-state electrochemical measurements were conducted on complex **1** for this purpose.

Solid-state electrochemical measurements were conducted in a variety of aqueous electrolyte systems upon mechanically attached crystals of complex **1**. In a range of 1 M aqueous electrolyte systems, such as $LiClO_4$, the POM exhibited only a clear redox wave associated with the $Fe^{III/II}$ couple of the $[Fe(bpy)_3]^{2+}$ moiety. To view any redox activity for the $[PW_{11}O_{39}Fe_2^{III}(OH)bpy)_2]^{2-}$ POM, the attached microcrystals were cycled electrochemically in a range of aqueous buffer solutions from pH 2 to 4. In pH 4, the presence of what is believed to be a monoelectronic wave at $E_{1/2} = -0.140$ V and associated with the $Fe^{III/II}$ within the Keggin cage is observed. In addition, two bielectronic waves associated with the reduction of the tungsten–oxo framework with $E_{1/2}$ values of −0.590 and −0.834 V, are clearly seen in Figure 7a. The last two waves were found to be pH-dependent in nature. This dependence is known for the redox activity of the tungsten–oxo processes for the polyoxotungstates in solution.[43] Shifts of 65 to 75 mV per decade change in pH were observed for both of these waves, thereby indicating the addition of two H^+ during each reduction step. This is similar to the unfunctionalized Fe^{III} Keggin POM. Scanning in a positive direction in these buffer solutions revealed the monoelectronic wave associated with the $Fe^{III/II}$ of the cationic $[Fe(bpy)_3]^{2+}$ moiety, with a pH-independent $E_{1/2}$ of +0.774 V (Figure 7b). The solid-state behavior of this com-

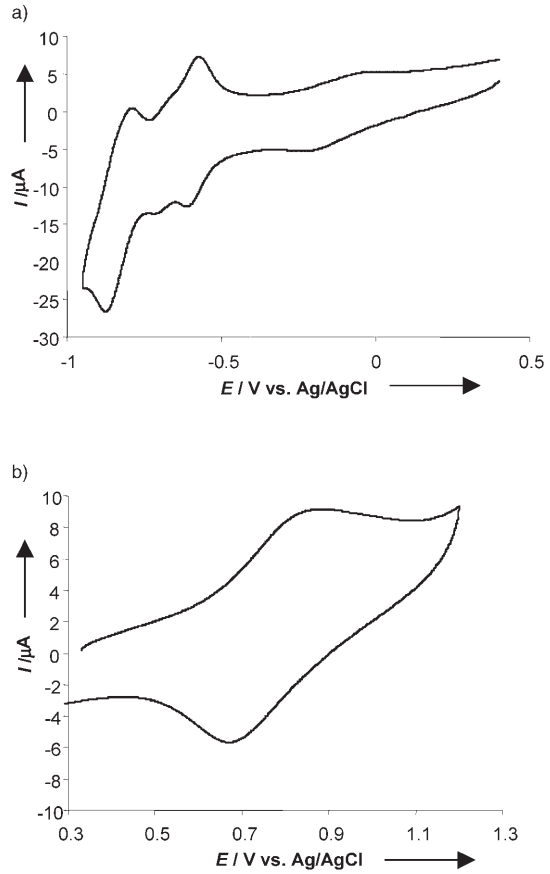

Figure 7. Solid state cyclic voltammograms of crystals of complex **1** adhered to a carbon electrode ($A = 0.0707\ cm^2$) in buffer pH 4 solution a) in the −1.0 to 0.0 V range; b) in the 0.0–1.3 V range. Scan rate = $100\ mV\,s^{-1}$.

plex agrees well with the electrochemical properties of the $[Fe(bpy)_3]^{2+}$ and $[PW_{11}O_{39}Fe^{III}(H_2O)]^{4-}$ salts under the same conditions with little shift in redox potentials.

The insolubility of complex **2** curtailed the investigation of the solution phase electrochemistry of this complex. As a result, the solid-state electrochemical behavior of complex **2** was investigated in buffered solutions so as to view the redox activity of this complex. In a pH 2 buffer, the attached microcrystals of complex **2** exhibited two bielectronic W–O processes with $E_{1/2}$ values of −0.410 and −0.645 V, and two redox couples at +0.044 V and +0.768 V, as seen in Figure SI5 in the Supporting Information. The latter being due to the redox switching of the Fe^{II} in the $[Fe^{II}(dmbpy)_3]^{2+}$ cation, and the former is due to the Fe^{III} centers within the POM itself. The number of electrons involved in each process is difficult to ascertain due to the complex's inherent insolubility.

Conclusion

The synthesis of $[PW_{11}O_{39}Fe_2^{III}(OH)(bpy)_2]^{2-}$, $[(PW_{11}O_{39})_2Fe_4^{III}O_2(dmbpy)_4]^{6-}$, and $[(PW_{11}O_{39})_2Fe_2^{III}O]^{10-}$ shows that hydrothermal conditions can be efficiently used for the synthesis of magnetic clusters encapsulated in POMs starting from vacant polyoxotungstate precursors. To date, the reaction of $[PW_{11}O_{39}]^{7-}$ towards first-row transition-metal ions M^{n+} under normal bench conditions has only led to monosubstituted $\{PW_{11}O_{39}M(H_2O)\}$ anions, in which M is disordered over the twelve metallic centers. Hydrothermal conditions enhance the reactivity of the monolacunary precursor and allow the isolation of more sophisticated species. Notably, the use of bipyridine-type ligands allowed an asymmetric dinuclear {Fe(μ-O(W))(μ-OH)Fe}-containing complex in which one iron atom is coordinated to a monovacant POM, while the other is coordinated to two bipyridine ligands to be obtained, and a hybrid centrosymetric compound in which a tetranuclear Fe_4 core is sandwiched between two POMs was also isolated. The latter complex represents, to our knowledge, the first characterized butterfly-like POM cluster. When non-coordinating tetramethylammonium cations replace bipyridine ligands in the synthetic process, the hydrothermal conditions allowed the isolation of a purely inorganic dinuclear Fe(μ-O)Fe cation in which the magnetic core is sandwiched between two POMs. For the three compounds, the antiferromagnetic coupling constants between the paramagnetic centers have been determined and compared with related non-POM compounds. Particularly, this comparison combined with DFT calculations has confirmed that metallic centers bridged by an oxo ligand from the POM are weakly coupled. This is due to long distances between the magnetic center and the oxygen atom of the POM, but also to the important mixing of bridging oxygen orbitals with the orbitals of the POM tungsten atoms. Electrochemical experiments on the hybrid complexes have allowed a partial determination of the redox waves associated with the metallic centers and the bipyridine ligands constituting complexes **1** and **2**. Our attention focuses now on other lacunary precursors as building units in order to increase the nuclearity of the magnetic clusters.

Experimental Section

Synthesis: $K_7[\alpha\text{-}PW_{11}O_{39}]\cdot 14H_2O$ was prepared according to a published procedure.[44] The hydrothermal syntheses were carried out in polytetrafluoroethylene-lined stainless steel containers under autogeneous pressure. The 23 mL vessel was filled to approximately 25% volume capacity ($V_i = 6$ mL). All reactants were stirred briefly before heating. The samples were heated for 60 h at 160 °C and cooled to room temperature over a period of 40 h. The pH mixture was measured before (pH_i) and after the reaction (pH_f). The products were isolated by filtration and washed with ethanol.

$[Fe^{II}(bpy)_3][PW_{11}O_{39}Fe_2^{III}(OH)(bpy)_2]\cdot 12H_2O$ (1): A mixture of $K_7[\alpha\text{-}PW_{11}O_{39}]\cdot 14H_2O$ (0.550 g, 0.175 mmol), $Fe_2(SO_4)_3$ (0.103 g, 0.257 mmol), 2,2′-bpy (0.135 g, 0.864 mmol), and H_2O (6 mL) was stirred and the pH was adjusted to 3 with 2 M KOH ($pH_f = 2$). Dark red parallelepipedic crystals (0.360 g, 58% yield based on W) were collected by filtration. The crystals were purified by heating (50 °C) gently in water in order to remove water soluble orange crystals which co-crystallized in small quantities with complex **1**. IR (KBr pellets): $\tilde{\nu} = 3116$ (w), 3046 (w), 2921 (w), 2851 (w), 1471 (m), 1443 (s), 1383 (w), 1316 (w), 1265 (w), 1245 (w), 1174 (sh), 1157 (w), 1066 (m), 1027 (w), 993 (sh), 959 (m), 880 (m), 817 (s),

798 (sh), 761 (sh), 730 (w), 690 (w), 670 (sh), 650 (w), 591 (w), 549 (w), 512 cm^{-1} (m); elemental analysis calcd (%) for $C_{50}H_{65}N_{10}Fe_3O_{52}PW_{11}$ (3858.85): C 15.56, H 1.69, N 3.63, Fe 4.34, P 0.80, W 52.40; found: C 15.92, H 1.27, N 3.73, Fe 4.63, P 0.87, W 52.20.

$(Hdmbpy)_2[Fe^{II}(dmbpy)_3]_2[(PW_{11}O_{39})_2Fe_4^{III}O_2(dmbpy)_4]\cdot 14H_2O$ (2): A mixture of $K_7[\alpha\text{-}PW_{11}O_{39}]\cdot 14H_2O$ (0.550 g, 0.175 mmol), $Fe_2(SO_4)_3$ (0.103 g, 0.257 mmol), 5,5′-dimethyl-2,2′-bpy (0.140 g, 0.760 mmol), and H_2O (6 mL) was stirred and the pH was adjusted to 3 with 2 M KOH ($pH_f = 3$). Dark red parallelepipedic crystals (0.360 g, 57% yield based on W) were collected by filtration. IR (KBr pellets): $\tilde{\nu} = 3120$ (w), 3100 (w), 3080 (w), 3060 (w), 3045 (w), 2921 (w), 2855 (w), 1475 (m), 1447 (w), 1382 (w), 1311 (w), 1240 (m), 1235 (sh), 1149 (m),1084 (sh), 1064 (m), 958 (m), 885 (m), 808 (s), 729 (m), 701 (w), 666 (w), 652 (sh), 582 (m), 524 (m), 504 cm^{-1} (sh); elemental analysis calcd (%) for $C_{144}H_{174}N_{24}Fe_6O_{94}P_2W_{22}$ (8186.56): C 21.13, H 2.14, N 4.10, Fe 4.09, P 0.76, W 49.40; found: C 20.56, H 1.88, N 3.84, Fe 3.95, P 0.73, W 47.92.

$H_2[Fe^{II}(dmbpy)_3]_2[(PW_{11}O_{39})_2Fe_4^{III}O_2(dmbpy)_4]\cdot 10H_2O$ (3): A mixture of $K_7[\alpha\text{-}PW_{11}O_{39}]\cdot 14H_2O$ (0.550 g, 0.175 mmol), $Fe_2(SO_4)_3$ (0.103 g, 0.257 mmol), 5,5′-dimethyl-2,2′-bpy (0.080 g, 0.434 mmol), and H_2O (6 mL) was stirred and the pH was adjusted to 3 with 2 M KOH ($pH_f = 3$). Dark red parallelepipedic crystals (0.150 g, 22% yield based on W) were collected by filtration. IR (KBr pellets): $\tilde{\nu} = 3120$ (w), 3100 (w), 3080 (w), 3060 (w), 3045 (w), 2921 (w), 2855 (w), 1475 (m), 1447 (w), 1382 (w), 1311 (w), 1240 (m), 1235 (sh), 1149 (m),1084 (sh), 1064 (m), 958 (m), 885 (m), 808 (s), 729 (m), 701 (w), 666 (w), 652 (sh), 582 (m), 524 (m), 504 cm^{-1} (sh); elemental analysis calcd (%) for $C_{120}H_{142}N_{20}Fe_6O_{90}P_2W_{22}$ (7746.03) C 18.61, H 1.85,N 3.62, Fe 4.33, P 0.80, W 52.21; found: C 19.55, H 1.75, N 3.78, Fe 4.38, P 0.81, W 50.85.

$[N(CH_3)_4]_{10}[(PW_{11}O_{39})_2Fe_2^{III}O]\cdot 12H_2O$ (4): A mixture of $K_7[\alpha\text{-}PW_{11}O_{39}]\cdot 14H_2O$ (0.550 g, 0.175 mmol), $Fe_2(SO_4)_3$ (0.103 g, 0.257 mmol), tetramethylammonium bromide (0.135 g, 0.878 mmol), and H_2O (6 mL) was stirred and the pH was adjusted to 4 with 2 M KOH ($pH_f = 2.5$). Parallelepipedic yellow crystals (0.310 g, 56% yield based on W) were collected by filtration. IR (KBr pellets): $\tilde{\nu} = 3034$ (m), 2958 (w), 2922 (w), 2854 (w), 2768(w), 2763 (w), 2655 (w), 2589 (w), 2519 (w), 2487 (w), 1629 (w), 1486 (s), 1450 (m), 1418 (m), 1384 (m), 1286 (m), 1262 (m), 1093 (sh), 1057 (m), 956 (s), 815 (s), 759 (w), 729 (sh), 690 (w), 668 (sh), 595 (m), 521 (w), 489 (sh), 456 (m), 412 cm^{-1} (m); elemental analysis calcd (%) for $C_{40}H_{144}N_{10}Fe_2O_{91}P_2W_{22}$ (6439.73) C 7.46, H 2.25,N 2.17, Fe 1.73, P 0.96, W 62.80; found: C 7.47, H 2.11, N 2.15, Fe 1.72, P 1.01, W 60.76.

X-ray crystallography: The intensity data collection for complexes **1–4** was carried out using a Bruker Nonius X8 APEX 2 diffractometer equipped with a CCD bidimensional detector with the monochromated radiation ($\lambda(Mo_{K\alpha}) = 0.71073$ Å). All the data were recorded at room temperature. The absorption correction was based on multiple and symmetry-equivalent reflections in the data set using the SADABS program[45] based on the Blessing's method.[46] The structures were solved by using direct methods and refined by full-matrix least-squares methods with the SHELX-TL package.[47] In all the structures, there is a discrepancy between the formulae determined by elemental analysis and the formulae deduced from the crystallographic atom list, because of the difficulty in locating all the disordered water molecules. These molecules have been refined with partial occupancy factors. In the structure of complex **2**, it has been possible to locate the free $Hdmby^+$ ions, the assignment of the two N atom positions among the four possible ones was made by considering the distances. The structure of complex **3** was solved in the noncentrosymmetric *P*1 space group, although an analysis by Platon suggests $P\bar{1}$ because, in the centrosymmetric space group, the bpy ligands were too close in space. Crystallographic data are given in Table 2. Selected bond lengths and angles are listed in Table 1. CCDC 649965 (**1**), 649966 (**2**), 649967 (**3**) and 649968 (**4**) contain the supplementary crystallographic data for this paper. These data can be obtained free of charge from The Cambridge Crystallographic Data Centre via www.ccdc.cam.ac.uk/data_request/cif.

TGA measurements: Thermogravimetry was carried out in a N_2/O_2 (1:1) flow (60 mL min^{-1}) with a Perkin–Elmer electrobalance TGA-7 at a heating rate 10 °C min^{-1} up to 800 °C.

Magnetic measurements: Magnetic susceptibility measurements were carried out with a Quantum Design SQUID Magnetometer with an applied field of 1000 Oe using powder samples pressed in pellets to avoid preferential orientation of the crystallites. The independence of the susceptibility value with regard to the applied field was checked at room temperature. The susceptibility data were corrected from the diamagnetic contributions as deduced by using Pascal's constant tables. 4.85, 4.07, and 0.04% of paramagnetic Fe^{III} impurities were taken into account for the fit of complexes **1**, **2**, and **4**, respectively.

Computational details: Electronic structure calculations were performed with the GAUSSIAN 03 package.[48] The Fe and W atoms were described using LANL2DZ basis set with LANL2 effective core potentials, whereas the 6–31g basis set was used for all other atoms. The three-parameter exchange-correlation functional of Becke based on the correlation functional of Lee, Yang, and Parr (B3LYP),[49] which is known to be suited for

Table 2. X-ray crystallographic data for complexes **1–4**.

	1	**2**	**3**	**4**
formula	$C_{50}H_{45}Fe_3N_{10}O_{52}PW_{11}$	$C_{144}H_{146}Fe_6N_{24}O_{81}P_2W_{22}$	$C_{120}H_{120}Fe_6N_{20}O_{81}P_2W_{22}$	$C_{40}H_{144}Fe_2N_{10}O_{91}P_2W_{22}$
M_r	3838.83	7950.59	7580.10	6439.73
crystal system	monoclinic	monoclinic	triclinic	triclinic
space group	*C*2/*c*	*C*2/*c*	*P*1	$P\bar{1}$
Z	8	4	1	2
T [K]	293	293	293	293
a [Å]	23.1859(8)	28.851(2)	13.3562(6)	13.1534(3)
b [Å]	13.9166(8)	36.971(3)	14.1707(6)	20.3426(6)
c [Å]	47.537(2)	20.947(2)	24.778(1)	24.0622(7)
α [°]	90	90	81.004(2)	94.2950(10)
β [°]	103.247(4)	118.229(4)	83.810(2)	97.1150(10)
γ [°]	90	90	65.434(2)	92.1570(10)
V [Å^3]	14931(1)	19686(3)	4207.9(3)	6363.7(3)
ρ_{calcd} [g cm^{-3}]	3.416	2.683	2.991	3.361
μ [mm^{-1}]	17.573	13.325	15.576	20.136
reflns collected	71279	75101	76836	160858
unique reflns (R_{int})	22050(0.0720)	17344(0.1581)	37765(0.0508)	37375(0.0472)
refined parameters	1029	1072	2178	1342
$R(F_o)$[a]	0.0701	0.0653	0.0610	0.0657
$R_w(F_o^2)$[b]	0.1758	0.1587	0.1576	0.1153

[a] $R_1 = [\Sigma\,|\,|F_o| - |F_c|\,|]/\Sigma\,|F_c|$;[b] $wR_2 = \{[\Sigma w(F_o^2 - F_c^2)^2]/\Sigma w(F_o^2)^2\}^{1/2}$ with $1/w = \sigma^2 F_o^2 + aP^2 + bP$ and $P = (F_o^2 + F_c^2)/3$; $a = 0.0991$, $b = 601.63$ for **1**; $a = 0.1195$, $b = 0$ for **2**; $a = 0.1160$, $b = 0$ for **3**; $a = 0.0795$, $b = 272.69$ for **4**.

the estimation of exchange interactions, was used in all calculations. The exchange parameters were evaluated following the DFT-broken symmetry method.[50]

Electrochemical measurements: The reference electrode employed in organic solvents was a silver wire in contact with a solution of $AgNO_3$ (0.01 M) and 0.1 M of the same supporting electrolyte as employed in the cell. For aqueous electrochemistry a silver/silver chloride (3 M KCl) reference electrode was used. A carbon ($d=3$ mm) working electrode was employed which was polished prior to use with 0.05 μm alumina and rinsed with deionized water. The auxiliary electrode material was a platinum wire. A CH 660 A potentiostat was employed for all electrochemical experiments. All solutions were degassed with pure argon for 15 min prior to electrochemical experiments. For solid-state voltammetric measurements, a slurry of the complexes was first prepared and then transferred onto the electrode surface. Before the electrochemical studies, the coatings were allowed to dry. After use, the electrode surface was renewed by rinsing with acetone, polishing with 0.05 μm alumina and then sonicated in deionized water.

[1] M. T. Pope, *Heteropoly and Isopoly Oxometalates*, Springer, Berlin, **1983**.
[2] D.-L. Long, E. Burkholder, L. Cronin, *Chem. Soc. Rev.* **2007**, *36*, 105.
[3] B. Godin, Y.-G. Chen, J. Vaissermann, L. Ruhlmann, M. Verdaguer, P. Gouzerh, *Angew. Chem.* **2005**, *117*, 3132; *Angew. Chem. Int. Ed.* **2005**, *44*, 3072.
[4] a) A. Müller, F. Peters, M. T. Pope, D. Gatteschi, *Chem. Rev.* **1998**, *98,* 240; b) J. M. Clemente-Juan, E. Coronado, *Coord. Chem. Rev.* **1999**, *193–195*, 361.
[5] See for example the recent special issue on POMs: *J. Mol. Catal. A* **2007**, *262*, 1–242.
[6] P. Mialane, A. Dolbecq, F. Sécheresse, *Chem. Commun.* **2006**, *33*, 3477.
[7] a) P.-Q. Zheng, Y.-P. Ren, L.-S. Long, R.-B. Huang, L.-S. Zheng, *Inorg. Chem.* **2005**, *44*, 1190; b) H. Jin, C. Qin, Y.-G. Li, E.-B. Wang, *Inorg. Chem. Commun.* **2006**, *9*, 482; c) X.-J. Kong, Y.-P. Ren, P.-Q. Zheng, Y.-X. Long, L.-S. Long, R.-B. Huang, L.-S. Zheng, *Inorg. Chem.* **2006**, *45*, 10702.
[8] C. Ritchie, E. Burkholder, P. Kögerler, L. Cronin, *Dalton Trans.* **2006**, 1712.
[9] S.-T. Zheng, D.-Q. Yuan, H.-P. Jia, J. Zhang, G.-Y. Yang, *Chem. Commun.* **2007**, 1858.
[10] a) R. N. Devi, E. Burkholder, J. Zubieta, *Inorg. Chim. Acta* **2003**, *348*, 150; b) L. Lisnard, A. Dolbecq, P. Mialane, J. Marrot, F. Sécheresse, *Inorg. Chim. Acta* **2004**, *357*, 845.
[11] a) Y. Xu, J.-Q. Xu, K.-L. Zhang, Y. Zhang, X.-Z. You, *Chem. Commun.* **2000**, 153; b) B. Yan, Y. Xu, X. Bu, N. K. Goh, L. S. Chia, G. D. Stucky, *J. Chem. Soc. Dalton Trans.* **2001**, 2003; c) E. Burkholder, V. Golub, C. J. O'Connor, J. Zubieta, *Inorg. Chem. Commun.* **2004**, *7*, 363; d) L. Lisnard, A. Dolbecq, P. Mialane, J. Marrot, E. Codjovi, F. Sécheresse *Dalton Trans.* **2005**, 3913.
[12] J.-P. Wang, Q. Ren, J.-W. Zhao, J.-Y. Niu, *Inorg. Chem. Commun.* **2006**, *9*, 1281.
[13] L. S. Felices, P. Vitoria, J. M. Gutiérrez-Zorrilla, L. Lezama, S. Reinoso, *Inorg. Chem.* **2006**, *45*, 7748.
[14] S. Chang, C. Qin, E. Wang, Y. Li, X. Wang, *Inorg. Chem. Commun.* **2006**, *9*, 727.
[15] a) L.-H. Bi, U. Kortz, S. Nellutla, A. C. Stowe, J. v. Tol, N. S. Dala, B. Keita, L. Nadjo, *Inorg. Chem.* **2005**, *44*, 896; b) M. Prinz, A. F. Takács, J. Schnack, I. Balasz, E. Burzo, U. Kortz, K. Kuepper, M. Neumann, *J. Appl. Phys.* **2006**, *99*, 08J505.
[16] a) U. Kortz, M. G. Savelieff, B. S. Bassil, B. Keita, L. Nadjo, *Inorg. Chem.* **2002**, *41*, 783; b) B. Keita, I. M. Mbomekalle, L. Nadjo, T. M. Anderson, C. Hill, *Inorg. Chem.* **2004**, *43*, 3257.
[17] a) T. M. Anderson, X. Zhang, K. I. Hardcastle, C. Hill, *Inorg. Chem.* **2002**, *41*, 2477; b) N. M. Okun, T. M. Anderson, C. Hill, *J. Am. Chem. Soc.* **2003**, *125*, 3194; c) B. Botar, Y. V. Geletii, P. Kögerler, D. G. Musaev, K. Morokuma, I. A. Weinstock, C. Hill, *J. Am. Chem. Soc.* **2006**, *128*, 11268; d) M. Bonchio, M. Carraro, A. Sartorel, G. Scorrano, U. Kortz, *J. Mol. Catal. A* **2007**, *262*, 36; e) I. C. M. S. Santos, J. A. F. Gamelas, M. S. S. Balula, M. M. Q. Simoes, M. G. P. M. S. Neves, J. A. S. Cavaleiro, A. M. V. Cavaleiro, *J. Mol. Catal. A* **2007**, *262*, 41.
[18] a) N. Mizuno, K. Yamaguchi, K. Kamata, *Coord. Chem. Rev.* **2005**, 249; b) M. Bonchio, M. Carraro, A. Sartorel, G. Scorrano, U. Kortz, *J. Mol. Catal. A* **2006**, *251*, 93.
[19] $a=13.3642(2)$, $b=17.2873(3)$, $c=20.3975(4)$ Å, $\alpha=90$, $\beta=77.604(1)$, $\gamma=90°$, $V=4602.6$ Å^3.
[20] J. R. Galán-Mascarós, C. Giménez-Saiz, S. Triki, C. J. Gómez-Garcia, E. Coronado, L. Ouahab, *Angew. Chem.* **1995**, *107*, 1601; *Angew. Chem. Int. Ed. Engl.* **1995**, *34*, 1460.
[21] B. Yan, Y. Xu, X. Bu, N. K. Goh, L. S. Chia, G. D. Stucky, *J. Chem. Soc. Dalton Trans.* **2001**, 2009.
[22] a) F. Zonnevijlle, C. M. Tourné, G. F. Tourné, *Inorg. Chem.* **1982**, *21*, 2742; b) J. A. Gamelás, F. A. A. Couto, M. N. Trovão, A. M. V. Cavaleiro, J. A. S. Cavaleiro, J. D. Pedrosa de Jesus, *Thermochim. Acta* **1999**, *326*, 165.
[23] F. Zonnevijlle, C. M. Tourné, G. F. Tourné, *Inorg. Chem.* **1982**, *21*, 2751.
[24] a) Z.-E. Lin, J. Zhang, Y.-Q. Sun, G.-Y. Yang, *Inorg. Chem.* **2004**, *43*, 797; b) W. Yang, C. Lu, *Inorg. Chem.* **2002**, *41*, 5638; c) L. Lisnard, A. Dolbecq, P. Mialane, J. Marrot, E. Rivière, S. A. Borshch, S. Petit, V. Robert, C. Duboc, T. McCormac, F. Sécheresse, *Dalton Trans.* **2006**, 5141.
[25] P. A. Lay, W. H. F. Sasse, *Inorg. Chem.* **1985**, *24*, 4707.
[26] N. E. Brese, M. O'Keeffe, *Acta Crystallogr. Sect. B* **1991**, *47*, 192.
[27] a) J. K. McCusker, J. B. Vincent, E. A. Schmitt, M. L. Mino, K. Shin, D. K. Coggin, P. M. Hagen, J. C. Huffman, G. Christou, D. N. Hendrickson, *J. Am. Chem. Soc.* **1991**, *113*, 3012; b) A. K. Boudalis, N. Lalioti, G. A. Spoyroulias, C. P. Raptopoulou, A. Terzis, A. Bousseksou, V. Tangoulis, J.-P. Tuchagues, S. P. Perlepes, *Inorg. Chem.* **2002**, *41*, 6474; c) J. Overgaard, D. E. Hibbs, E. Rentschler, G. A. Timco, F. K. Larsen, *Inorg. Chem.* **2003**, *42*, 7593; d) T. C. Stamatatos, A. K. Boudalis, Y. Sanakis, C. P. Raptopoulou, *Inorg. Chem.* **2006**, *45*, 7372.
[28] J. M. Clemente-Juan, E. Coronado, *Coord. Chem. Rev.* **1999**, 361.
[29] R. G. Finke, M. Droege, J. R. Hutchinson, O. Gansow, *J. Am. Chem. Soc.* **1981**, *103*, 1587; T. J. R. Weakley, R. G. Finke, *Inorg. Chem.* **1990**, *29*, 1235; C. J. Gómez-García, E. Coronado, P. Gómez-Romero, N. Casañ-Pastor, *Inorg. Chem.* **1993**, *32*, 3378; X.-Y. Zhang, G. B. Jameson, C. J. O'Connor, M. T. Pope, *Polyhedron* **1996**, *15*, 917.
[30] X. Zhang, Q. Chen, D. C. Duncan, R. J. Lachicotte, C. Hill, *Inorg. Chem.* **1997**, *36*, 4381.
[31] F. Zonnevijlle, C. M. Tourné, G. F. Tourné, *Inorg. Chem.* **1982**, *21*, 2751.
[32] O. A. Kholdeeva, G. M. Maksimov, R. I. Maksimovskaya, L. A. Kovalena, M. A. Fedotov, V. A. Grigoriev, C. L. Hill, *Inorg. Chem.* **2000**, *39*, 3828.
[33] O. A. Kholdeeva, G. M. Maksimov, R. I. Maksimovskaya, P. Vanina, T. A. Trubitsina, D. Yu Naumov, B. A. Kolesov, N. S. Antonova, J. J. Carbó, J. M. Poblet, *Inorg. Chem.* **2006**, *45*, 7224.
[34] a) M. Sadakane, M. Higashijima, *Dalton Trans.* **2003**, 659; b) M. Sadakane, D. Tsukuma, M. H. Dickman, B. S. Bassil, U. Kortz, M. Capron, W. Ueda, *Dalton Trans.* **2007**, 2833.
[35] $R=[\Sigma(\chi_M T_{calc}-\chi_M T_{obs})^2/\Sigma(\chi_M T_{obs})^2]$
[36] a) D. M. Kurtz, *Chem. Rev.* **1990**, *90*, 585; b) E. I. Solomon, T. C. Brunold, M. I. Davis, J. N. Kemsley, S. K. Lee, N. Lehnert, F. Neese, A. J. Skulan, Y.-S. Yang, J. Zhou, *Chem. Rev.* **2000**, *100*, 235; c) E. Y. Tshuva, S. J. Lippard, *Chem. Rev.* **2004**, *104*, 987.
[37] A. Stubna, D.-H. Jo, M. Costas, W. W. Brenessel, H. Andres, E. L. Bominaar, E. Münck, L. Que, Jr., *Inorg. Chem.* **2004**, *43*, 3067.
[38] a) S. M. Gorun, S. J. Lippard, *Inorg. Chem.* **1991**, *30*,1625; b) H. Weihe, H. U. Güdel, *J. Am. Chem. Soc.* **1997**, *119*, 6539; c) R. Werner, S. Ostrovsky, K. Griesar, W. Haase, *Inorg. Chim. Acta*, **2001**, *326*, 78.

[39] J. Jullien, G. Juhász, P. Mialane, E. Dumas, C. R. Mayer, J. Marrot, E. Rivière, E. L. Bominaar, E. Münck, F. Sécheresse, *Inorg. Chem.* **2006**, *45*, 6922.
[40] T. Cauchy, E. Ruiz, S. Alvarez, *J. Am. Chem. Soc.* **2006**, *128*, 15722.
[41] A. Hazell, K. B. Jensen, C. J. McKenzie, H. Toftlund, *Inorg. Chem.* **1994**, *33*, 3127.
[42] E. M. Zueva, H. Chermette, S. A. Borshch, *Inorg. Chem.* **2004**, *43*, 2834.
[43] N. Fay, E. Dempsey, T. McCormac, *J. Electroanal. Chem.* **2005**, *574*, 359.
[44] R. Contant, *Can. J. Chem.* **1987**, *65*, 570.
[45] G. M. Sheldrick, SADABS, program for scaling and correction of area detector data, University of Göttingen, Göttingen (Germany), **1997**.
[46] R. Blessing, *Acta Crystallogr. Sect. A* **1995**, *51*, 33.
[47] G. M. Sheldrick, SHELX-TL version 5.03, software package for the crystal structure determination, Siemens Analytical X-ray Instrument Division, Madison, WI (USA), **1994**.
[48] Gaussian 03 (Revision C. 02), M. J. Frisch, G. W. Trucks, H. B. Schlegel, G. E. Scuseria, M. A. Robb, J. R. Cheeseman, J. A. Montgomery Jr., T. Vreven, K. N. Kudin, J. C. Burant, J. M. Millam, S. S. Iyengar, J. Tomasi, V. Barone, B. Mennucci, M. Cossi, G. Scalmani, N. Rega, G. A. Petersson, H. Nakatsuji, M. Hada, M. Ehara, K. Toyota, R. Fukuda, J. Hasegawa, M. Ishida, T. Nakajima, Y. Honda, O. Kitao, H. Nakai, M. Klene, X. Li, J. E. Knox, H. P. Hratchian, J. B. Cross, C. Adamo, J. Jaramillo, R. Gomperts, R. E. Stratmann, O. Yazyev, A. J. Austin, R. Cammi, C. Pomelli, J. W. Ochterski, P. Y. Ayala, K. Morokuma, G. A. Voth, P. Salvador, J. J. Dannenberg, V. G. Zakrzewski, S. Dapprich, A. D. Daniels, M. C. Strain, O. Farkas, D. K. Malick, A. D. Rabuck, K. Raghavachari, J. B. Foresman, J. V. Ortiz, Q. Cui, A. G. Baboul, S. Clifford, J. Cioslowski, B. B. Stefanov, G. Liu, A. Liashenko, P. Piskorz, I. Komaromi, R. L. Martin, D. J. Fox, T. Keith, M. A. Al-Laham, C. Y. Peng, A. Nanayakkara, M. Challacombe, P. M. W. Gill, B. Johnson, W. Chen, M. W. Wong, C. Gonzalez, J. A. Pople, Gaussian, Inc., Pittsburgh, PA, **2004**.
[49] a) C. T. Lee, W. T. Yang, R. G. Parr, *Phys. Rev. B* **1988**, *37*, 785; b) A. D. Becke, *J. Chem. Phys.* **1993**, *98*, 5648.
[50] a) L. Noodleman, J. G. Norman Jr, *J. Chem. Phys.* **1979**, *70*, 4903; b) L. Noodleman, *J. Chem. Phys.* **1981**, *74*, 5737.

Received: June 13, 2007
Revised: October 15, 2007
Published online: January 29, 2008

